PET Image Reconstruction with a Bayesian Projector for Multi-Electronic Collimation Schemes

Garry Chinn, and Craig S. Levin, *Member, IEEE*

***Abstract*–We evaluated a new image reconstruction algorithm using a Bayesian projector for multi-collimation PET systems. We are developing a PET system using high spatial and energy resolution 3-D detectors made from cadmium zinc telluride with cross-strip anodes and cathodes. This PET system can collimate photon pairs by coincidence timing and can collimate single photons by the kinematics of Compton scatter within the detector (Compton collimation). Compton collimation of single photons can dramatically increase overall photon sensitivity by making use of events that are discarded by conventional PET systems. However, single photon events offer lower spatial resolution than coincidence measurements. Previously, we showed that conventional maximum likelihood reconstruction by the list-mode ordered subset expectation-maximization (OS-EM) algorithm for these "multi-collimation" data sets yields no measurable improvement over images reconstructed using high-resolution coincidence collimation alone. We also studied a Bayesian projector function with non-uniform emission probability along the line of response weighted by an image prior generated from the low-resolution (Compton collimation) channel, to reconstruct the high-resolution (coincidence) channel. In this work, we investigated a novel approach using priors generated by reconstructing images from the high-spatial resolution coincidence data followed by post-reconstruction smoothing with a new spatially varying 3-D filter function and the Perona-Malik gradient anisotropic diffusion filter.**

I. Introduction

Multi-collimation PET systems employ multiple methods of collimation with varying spatial resolution. One example is an insert system [1], [2], which places high spatial resolution detectors inside a conventional PET system with collimation channels formed by coincidences between the different detector rings. Another example is a PET system using 3D cadmium zinc telluride (CZT) detectors [3], [4], which can measure coincidence events and also use Compton kinematics to collimate single photons. In typical PET systems, there are significantly more single photon events than coincidence photons. By reconstructing images with coincidence and single photons, higher effective photon sensitivity and reconstructed signal-to-noise ratio is possible. Compton kinematics, illustrated in Fig. 1, can be performed when a photon undergoes one or more Compton interactions in the detector. With current detector technology, angular blurring of the Compton collimation direction leads to lower spatial resolution than standard coincidence photon collimation.

Maximum likelihood estimation (MLE) can be used to reconstruct PET images for these *multi-collimation* schemes. MLE effectively weights a combination of the collimation channels, such as single and coincidence photon, deconvolving the lower spatial resolution (single photon) channel to match the high-resolution (coincidence photon) channel. The weight of the low-resolution channel is proportional to the signal-to-noise after deconvolution. For sufficiently large resolution mismatch between channels, the low-resolution channel is effectively assigned a small weight and the MLE combination yields comparable spatial resolution and variance from images produced by using the high-resolution channel alone, while significantly improving the SNR. In our previous work, we have confirmed this result [3].

Here, we further refine the Bayesian projector method [3] by examining a new Bayesian prior. For evaluation purposes, we used Monte Carlo simulations of a multi-collimation PET scheme built using 3-D CZT detectors. However, this algorithm is applicable to any multi-collimation PET system.

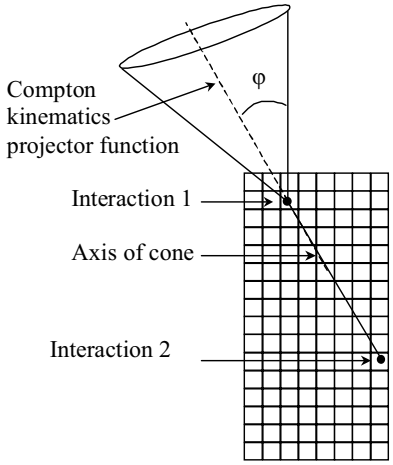

Fig 1. A schematic of Compton kinematics is shown for the 3-D CZT detector. The spatial location of two interactions in the detector determines the axis of the cone. The measured energy of the interactions determines the angle of the cone.

II. Method

In conventional image reconstruction, the emission probability is uniform along the line of response (LOR). In our Bayesian projector method, the probability along the LOR is weighted by a prior image – the LOR probability passing through regions of high activity in the prior will have high probability relative to regions of low activity in the prior. Previously, we used the low-spatial resolution Compton

Manuscript received November 15, 2007. This work was supported in part by the NIH under Grant Nos. NIBIB R33 EB003283, NCI R01 CA119056, NIH R01 CA120474 and also UCBCRP 121B-0092.

G. Chinn is with the Molecular Imaging Program at Stanford University and the Stanford School of Medicine, Stanford, CA 94305-5128 USA (telephone: 650-736-7218, e-mail: gchinn@stanford.edu).

C. S. Levin is with the Molecular Imaging Program at Stanford University and the Stanford School of Medicine, Stanford, CA 94305-5128 USA (telephone: 650-736-7211, e-mail: cslevin@stanford.edu).

Authorized licensed use limited to: Stanford University. Downloaded on May 21,2010 at 15:09:38 UTC from IEEE Xplore. Restrictions apply.

collimated single-photon channel to produce a prior for weighting the high-resolution coincidence photon channel [3] and showed a qualitative improvement in visual quality. In this work, a new reconstruction algorithm was used as depicted in Fig. 2. The list-mode OS-EM algorithm [5] was used to iteratively calculate the MLE solution. We generated priors from the higher resolution coincidence photon data for reconstructing the low-resolution single photon channel.

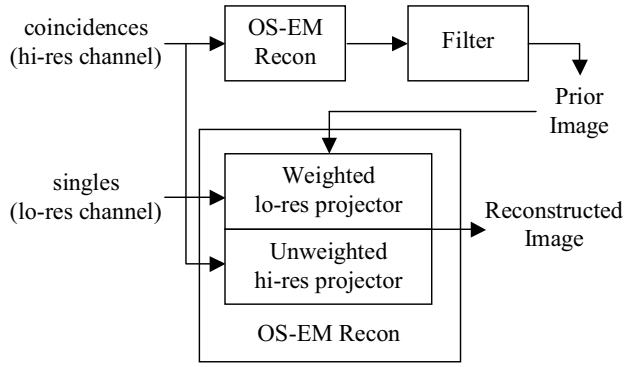

Fig. 2: A schematic of mutli-collimation image reconstruction using a Bayesian projector function is shown. The hi-resolution channel is used to generate a prior for weighting the projector function of the low-resolution channel. The image is reconstructed by using the 3D OS-EM reconstruction of both collimation channels simultaneously.

A. Creating a Prior

An image reconstructed from the coincidence photons was filtered to produce the prior. We investigated two different filtering approaches.

The first was a 3-D spatially-varying filter:

$$y(i,j,k) = \sum_l \sum_m \sum_n I_A(i,j,k,l,m,n) \cdot h(i-l, j-m, k-n)x(i-l, j-m, k-n) \quad (1)$$

where h is the filter kernel; x and y are the images before and after filtering, and the indicator function I_A is defined over the interval

$$A = \{|x(i,j,k) - x(i-l, j-m, k-n)| < \alpha\sqrt{x(i,j,k)} + \varepsilon\}. \quad (2)$$

The parameter α tunes the filtering to the expected lesion contrast. The image using both unweighted coincidences and weighted Compton collimation photons was produced by 1 iteration with 5 subsets of the 3D OS-EM algorithm (for 9:1 sphere:background ratio, 1.75 mm spheres).

A second filter was also used, a gradient anisotropic non-linear diffusion filter [6]. An iterative filter was created from a discrete diffusion equation. Each time step in the diffusion equation corresponded to an iteration of the filter. The total intensity of all pixels in the image was conserved at every time step with pixel intensity flowing to adjacent pixels. The diffusion rate and number of iterations can be used to control the degree of smoothness in the filtered image with more iterations and larger diffusion rates producing smoother images. The discrete diffusion equation is given by

$$\frac{u_{i,j}^{t+\Delta t} - u_{i,j}^t}{\Delta t} = \frac{1}{\Delta x}\left[E_{i,j}^t \nabla_E u_{i,j}^t - W_{i,j}^t \nabla_W u_{i,j}^t\right] + \frac{1}{\Delta y}\left[N_{i,j}^t \nabla_N u_{i,j}^t - S_{i,j}^t \nabla_S u_{i,j}^t\right] \quad (3)$$

where u is the intensity of the pixel at (i, j) at time step t. The diffusion coefficients in the north, east, south, and west directions are given by N, E, S, and W at pixel (i, j), respectively, take the form of

$$D_{i,j}^t = g\left(\left|\nabla_D u_{i,j}^t\right|^2\right) \quad (4)$$

where D specifies the direction (N, E, S, or W). The Perona-Malik filter [6] varies the diffusion coefficient, 1 within the interior of regions and 0 at the boundaries, in order to smooth the image while preserving edges.

B. Event Filtering for Compton Collimation

For Compton collimation, the lines of response form the surface of a cone as illustrated in Fig. 1. The measured energy of the first interaction is used to determine the photon angle φ relative to the cone axis, the line defined by the first two interactions. Uncertainty in the measured energy and the positioning of the cone axis leads to angular blurring. The angular blurring varies depending on the energy of the first scattering interaction and the distance between the interactions. Low-energy and high-energy interactions will have the poorest angular resolution. Also, the closer the two interactions are to each other, the worse the angular resolution.

Event filtering was used to improve the spatial resolution of Compton collimation. Since angular resolution degrades rapidly below a 15-20 degree scatter angle, single photons with detector scatter below 20 keV were not used to improve the angular resolution. A *minimum interaction distance threshold* was used to reduce the uncertainty of the cone axis position. Single photons were used only when the distance between the first two interactions were greater than 1 cm. At 1 cm separation between interactions, a 1 mm voxel size results in an angular error variance of 3 degrees if the discretization error is uniformly distributed. Event filtering improves angular resolution, but also reduces the single photon sensitivity.

C. Monte Carlo Simulation

An 8x8x2 cm^3 box-shaped system was simulated using CZT detectors as shown in Fig. 3. The CZT detectors were 4 x 4 x ½ cm^3 with cross-strip anodes and cathodes. This detector can position Compton scattering interactions within the detector in three dimensions with 1.5-2.5% FWHM at 511 keV energy resolution. Simulations were performed using an idealized energy resolution model

$$\Delta e = 0.025\sqrt{511e} \quad (5)$$

where e is the energy of the interaction in keV. This idealized energy resolution model assumes noiseless readout electronics. A more realistic model was also simulated, which assumed the readout electronics provided an additional 5 keV

Authorized licensed use limited to: Stanford University. Downloaded on May 21,2010 at 15:09:38 UTC from IEEE Xplore. Restrictions apply.

FWHM Gaussian noise source to each energy measurement independent of the interaction energy.

GRAY [7] was used to simulate two digital phantoms shown in Fig. 4. GRAY is Monte Carlo software that produces comparable results to those produced by GATE [7], [8] for CZT detectors in a fraction of the computation time. The phantoms were each 7.5 cm high by 3 cm diameter cylinders with 1, 1.25, 1.5, and 1.75 mm diameter spheres separated by twice the diameter organized in four different quadrants in the center slice of the cylinder. A total of 500 μCi total activity was scanned with 5 bed positions.

Phantom 1 was a 9 to 1 sphere-to-cylinder concentration ratio with idealistic energy resolution (5) and 30 sec. / bed position. After event filtering, 11 million Compton collimation single photons and 10 million coincidence photons were used for image reconstruction. A 10 ns coincidence time window and a 10% energy window at 511 keV for coincidence and single photons were used. The energy resolution of the CZT detector was 2.5% at 511 keV. Since multiple interactions can occur, the energy window was chosen to be larger than is conventionally used in PET.

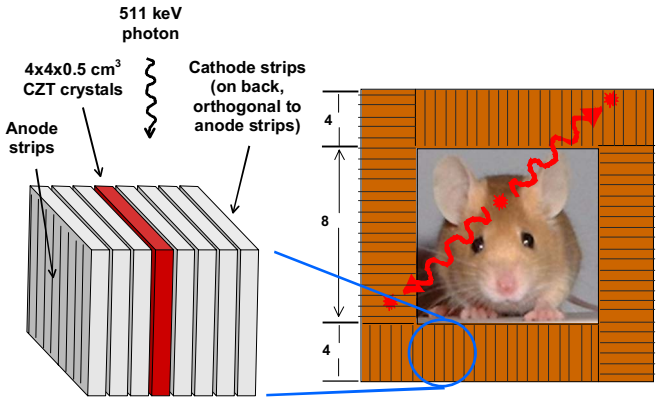

Fig. 3. Shown is a schematic of the small animal CZT system. The 4x4x1/2 cm^3 CZT detector has cross-strip anodes and cathodes and can position Compton scatter interactions in three dimensions. The detector is oriented in an edge-on configuration for higher sensitivity so that incoming photons see a minimum of 4 cm of CZT.

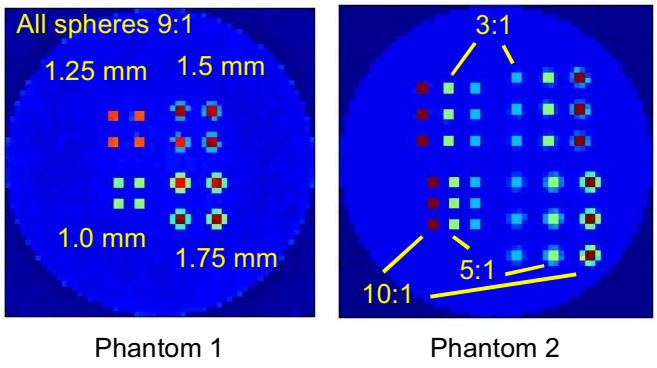

Fig. 4. Shown are the two digital phantoms used in the simulation study. Both phantoms are 7.5 cm high x 3 cm diameter cylinders with 1, 1.25, 1.5, and 1.75 mm spheres spaced at twice the diameter of the spheres. Phantom 1 has a 9 to 1 sphere-to-cylinder activity ratio. Phantom 2 has three columns of each size sphere. The outermost columns have a 9 to 1 sphere-to-cylinder activity ratio, the middle columns are 5 to 1, and the innermost are 3 to 1.

In phantom 2, the spheres are organized in three columns with 10 to 1, 5 to 1 and 3 to 1 sphere-to-cylinder activity ratio in the outer, middle, and inner columns, respectively. The scan time was 60 sec. per bed position using the more realistic energy resolution model. After event filtering, the simulation yielded 27 mil. Compton collimated single photon events and 21 mil. coincidence photons. Setting the minimum interaction distance threshold to zero, the number of available single events was 124 mil. So, event filtering reduced the number of usable single photon events by approximately 80%.

III. Results

A. Phantom 1 with Idealized Energy Blur Model

In Fig. 5, the reconstructed image from coincidence events for phantom 1 is shown on the left. Normalization/sensitivity correction was not used in the image reconstruction. The list-mode OS-EM algorithm was used with 2 iterations, 10 subsets per iteration. Subsets were divided by time with an equal number of counts for each subset. The right image was from combining coincidence and singles using 1 iteration, 5 subsets. The Bayesian prior was produced from coincidence data by using 5 iterations and 10 subsets/iteration. The filter described by (1) and (2) was used.

Using the Bayesian projector to reconstruct singles and coincidence events improved the SNR in a ROI drawn within the cylinder by a factor of 10 for similar recovered contrast of the spheres. The SNR in the spheres also improved by approximately 20% as measured by drawing ROIs in the center of every sphere.

B. Phantom 2 with More Realistic Energy Blur Model

For phantom 2, the reconstructed images with sensitivity correction are shown in Fig. 6. A Monte Carlo simulation with 30 minutes of simulated scan time was used to calculate the sensitivity correction. Gaussian smoothing was used. The image reconstructed from coincidence events is shown on the left. This image was produced by 2 iterations, 10 subsets per iteration. The image reconstructed using the Bayesian projector and 2 iterations, 6 subsets per iteration from combining coincidence and singles is shown on the right. The Bayesian prior was produced from coincidence data using 2 iterations, 10 subsets per iteration. The Perona-Malik filter was used for denoising the prior.

There was no significant improvement in the SNR for the spheres at comparable contrast as shown in Fig. 7. The SNR in the background cylinder ROI was improved by about 20%.

C. Effects of Detector Voxel Size

The detector voxel size was simulated at 0.025 mm, 0.5 mm, and 1.0 mm. The results of the sphere (lesion) SNR vs. contrast ratio for various iteration-subsets is shown in Fig. 8. There was no significant difference in reconstructed image quality for the various detector voxel sizes, suggesting that energy resolution was the dominant component of angular blurring for Compton collimation.

Authorized licensed use limited to: Stanford University. Downloaded on May 21,2010 at 15:09:38 UTC from IEEE Xplore. Restrictions apply.

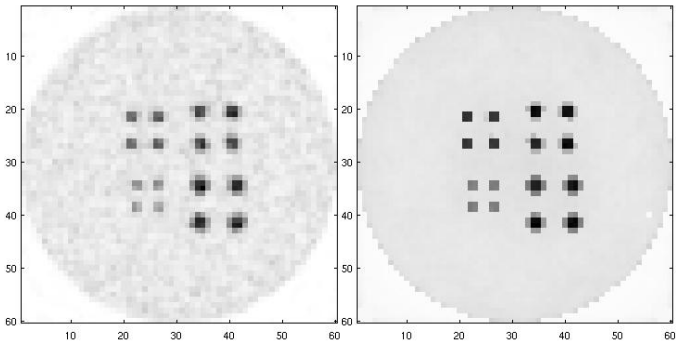

Fig. 5. Shown are the reconstructed images for phantom 1 (idealistic energy blur model). (Left) The OS-EM algorithm using only coincidence events was used to reconstruct the image with 2 iterations, 10 subsets per iteration. (Right) The list-mode OS-EM algorithm was used to combine coincidence and single photons with a single iteration and 5 subsets. The Bayesian projector was used for Compton collimation and the standard projector was used for coincidence events.

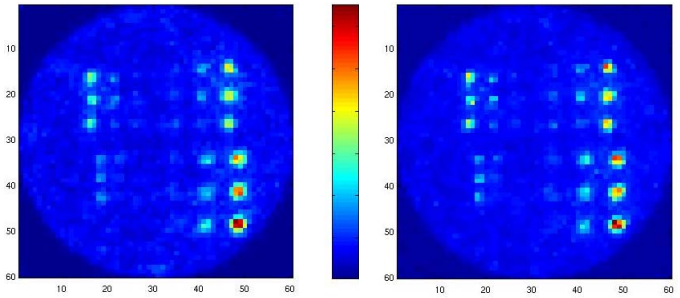

Fig. 6. Shown are the reconstructed images for phantom 2 with a more realistic energy resolution model. (Left) The OS-EM algorithm using coincidence events was used to reconstruct the image by 2 iterations, 10 subsets per iteration. (Right) The OS-EM algorithm using the Bayesian projector for Compton collimation and standard projector for coincidence events was used to reconstruct the image by 2 iteration, 6 subsets.

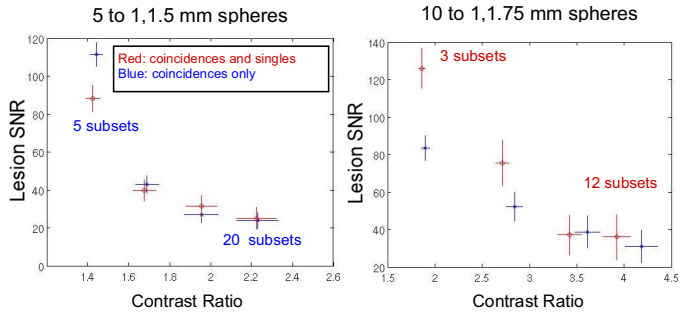

Fig. 7. Plots of sphere SNR vs. contrast ratio for different iteration-subsets are shown for coincidence reconstruction and combining coincidence and singles reconstruction using the Bayesian projector.

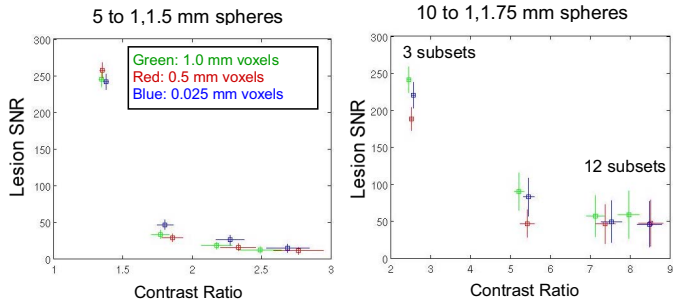

Fig. 8. Shown are plots of sphere SNR vs. contrast ratio for different iteration-subsets for coincidence and singles reconstruction using the Bayesian projector with detector voxel sizes of 0.025, 0.5, and 1 mm.

IV. Conclusions

For the ideal energy blur model, the Bayesian projector could combine single photons with coincidence photons to obtain images with better quality than could be achieved by using the coincidence data alone. For a more realistic energy blur model, there was no significant improvement to image quality from the addition of single photons over a range of lesion-background contrast. This study suggests that the angular resolution of Compton collimation must be improved in order to obtain benefits from imaging single photons.

An alternative detector design with air gaps between layers of CZT would likely improve the spatial resolution of Compton collimation. The average distance between interactions would increase, leading to a direct improvement in Compton collimation spatial resolution. Also, the number of interactions separated by more than 1 cm would increase significantly allowing the minimum interaction separation threshold to be increased, further improving spatial resolution.

The small animal system used in this study has high coincidence sensitivity and low single photon sensitivity. A human imaging system would have significantly higher relative single photon count rate and could yield improved image quality for combined coincidence and Compton collimation PET. With a large number of single photons, more aggressive event filtering could be used to improve Compton collimation spatial resolution.

Acknowledgment

We thank Peter Olcott for GRAY, which was used for Monte Carlo simulations.

References

[1] Y-C Tai, R. Laforest and A. Ruangma, "Design study of a detector insert for high-resolution clinical PET imaging," *Conf Proc.I EEE NSS-MIC, Portland*, 2003.

[2] D. Burdette, E. Chesi, N.H. Clinthorne, K. Honscheid, S.S. Huh, H. Kagen, C. Lacasta, G. Llosa, M. Mikuz, S.-J. Park, W.L. Rogers, A. Studen, P. Weilhammer, "First results from a test bench for very high resolution small animal PET using solid-state detectors," *IEEE NSS-MIC, Puerto Rico*, pp. 2376-2380, 2005.

[3] G. Chinn, A.M.K. Foudray and C.S. Levin, "A method to include single photon events in image reconstruction for a 1 mm resolution PET system built with advanced 3-D positioning detectors," *Conf. Proc. IEEE NSS-MIC, San Diego*, pp. 1740-1745, 2006.

[4] Levin CS, Mattesson JL, Skelton RT, Pelling MR, Duttweiler F, Huszar G, LeBlanc PC. Promising characteristics and performance of cadmium zinc telluride for positron emission tomography. *2004 Nuclear Science Symposium and Medical Imaging Conference*, Rome Italy, 2004. Abstract # M2-117, Book of Abstracts, p. 136, IEEE Nuclear and Plasma Science Society.

[5] H.M. Hudson and R.S. Larkin, "Accelerated image reconstruction using ordered subsets of projected data," *IEEE Trans. Med Imaging*, vol. 13, pp. 601-609, 1994.

[6] P. Perona, J. Malik, "Scale-space and edge detection using anisotropic diffusion," IEEE Trans. PAMI, vol. 12, no. 7, pp. 629-639, 1990.

[7] P.D. Olcott, S.R. Buss, C.S. Levin, G. Pratx, C.K. Sramek, "GRAY: high energy photon ray tracer for PET applications,"*Conf. Proc. IEEE NSS-MIC, San Diego*, pp. 2011-2015, 2006.

[8] S. Jan, et al., "GATE: a simulation toolkit for PET and SPECT," *Phys. Med. Biol.* vol. 49, 4543-4561, 2004.

Authorized licensed use limited to: Stanford University. Downloaded on May 21,2010 at 15:09:38 UTC from IEEE Xplore. Restrictions apply.